Applied Surface Science 358 (2015) 479–484

Contents lists available at ScienceDirect

Applied Surface Science

journal homepage: www.elsevier.com/locate/apsusc

Defect-mediated of Cu@TiO_2 core–shell nanoparticles with oxygen vacancies for photocatalytic degradation 2,4-DCP under visible light irradiation

Zhen Wang[a,b], Ling Zang[c], Xiaoyun Fan[a,*], Hanzhong Jia[a], Li Li[a,b], Wenye Deng[a], Chuanyi Wang[a,*]

[a] Laboratory of Environmental Sciences and Technology, Xinjiang Technical Institute of Physics & Chemistry, Key Laboratory of Functional Materials and Devices for Special Environments, Chinese Academy of Sciences, Urumqi 830011, China
[b] University of Chinese Academy of Sciences, Beijing 100049, China
[c] Department of Materials Science and Engineering, University of Utah, 122 S. Central Campus Drive, Salt Lake City, UT 84112, United States

ARTICLE INFO

Article history:
Received 8 June 2015
Received in revised form 5 August 2015
Accepted 6 August 2015
Available online 8 August 2015

Keywords:
Oxygen vacancies
Cu@TiO_2
Core–shell
Photocatalytic activity

ABSTRACT

Cu @TiO_2 core–shell nanoparticles with different mass ratios of Cu to TiO_2 were facilely synthesized via wet chemical approaches, and were characterized by transmission electron microscopy, scanning electron microscopy, UV–vis diffuse reflection absorption spectroscopy, X-ray photoelectron spectroscopy and electron paramagnetic resonance. The photocatalytic efficiency of Cu@TiO_2 nanoparticles was evaluated by degradation of 2,4-dichlorophenol, a typical persistent organic pollutant, under visible light irradiation. The results show that the oxygen vacancy creation obviously enhances the visible-light absorption of TiO_2. Meanwhile, the Cu nanoparticle incorporation into the TiO_2 can effectively improve charge-separation efficiency of Cu@TiO_2 under visible-light irradiation, thereby enhancing the photoactivity.

1. Introduction

As one of the most promising photocatalysts, TiO_2 has attracted significant attention due to its high photocatalytic activity, nontoxicity, physical and chemical stability. However, the high rate of photogenerated charge carriers recombination and the large band gap of TiO_2 result in the low quantum efficiency of photocatalytic reactions and the ineffective utilization of visible light or sunlight for TiO_2 which limit its usage in the visible light region [1–5]. It is known that couple noble metal with TiO_2 can greatly enhance the overall photocatalytic activity. Especially, heterostructures with metal core and TiO_2 shell not only have controllable chemical and colloidal stability within the shell but also charge effectively transfer between noble metal cores and TiO_2 [6,7]. Among all metals, copper as an important class of metal nanostructures has been increasingly studied due to its unusual properties and potential applications in thermal conducting, nanofluids and catalysts [8]. Compared to silver and gold, Cu behaves low price and stability at high frequencies, high-purity, uniformly shape and nanostructured, thus, Cu is highly desirable for use in microelectronics and catalysis [9–13].

Herein, we report for the first time on a new photocatalyst composed of Cu@TiO_2 core–shell nanoparticles, i.e., TiO_2 particles wrapped on copper nanoparticles. To assess the activity of the core–shell nanostructured photocatlyst, comparative studies on photodegradation of 2,4-dichlorophenol (DCP), a typical persistent organic pollutant, at core–shell nanostructured Cu@TiO_2 and its counter parts were conducted. Changing the concentration of $CuCl_2$ solution in the process of preparing Cu nanoparticles can tune the visible light responsibility of Cu@TiO_2. Moreover, the uniqueness of Cu@TiO_2 lies in the controllable chemical stability and effective charge transfer between Cu core and TiO_2 shell. In addition, the shell of TiO_2 can protect Cu against oxidation.

2. Experimental

2.1. Preparation of nanosized copper particles

Cu@TiO_2 samples were synthesized by a wet chemical approach. Cu nanoparticles were prepared by following a protocol developed by Xiong et al. [14]. 50 mL L-ascorbic acid aqueous solution (0.6 M) was added dropped into the $CuCl_2 \cdot 2H_2O$ solution (4.75 mM, 50 mL)

* Corresponding authors.
E-mail addresses: xyfan@ms.xjb.ac.cn (X. Fan), cywang@ms.xjb.ac.cn (C. Wang).

http://dx.doi.org/10.1016/j.apsusc.2015.08.051
0169-4332/

in an oil bath at 80 °C under magnetic stirring. Cu precipitates were obtained after 16 h reaction, then, separated by centrifugation, washed with absolute ethyl alcohol for three times.

2.2. Synthesis of Cu–core/TiO_2–shell nanoparticles

The wet Cu was dispersed into 50 mL of ethanol by ultrasonic treatment, and followed by dropwise addition of 118 mL of 0.03 M $Ti(OBu)_4$ ethanol solution under stirring. After 2 h, 116.5 mL mixed solution of water and absolute ethyl alcohol (volume ratio of water/absolute ethyl alcohol was 0.11) was dropped into the mixture, and the reaction was kept stirring at 300 rpm for another 2 h. The resulted composites were centrifuged, washed thoroughly with absolute ethanol and deionized water in sequence then dried at room temperature. As characterized below, the composite material thus prepared consists of mostly core–shell nanoparticles. Using the same protocol, a series of samples were prepared by changing the concentration of added $CuCl_2$ solution. The actual mass ratio of TiO_2 to Cu in Cu@TiO_2 composites under different concentrations of $CuCl_2$ was determined by atomic absorption spectroscopy. In the present work, Samples with mass ratios of 1.53%, 1.27%, 1.07%, 0.86% and 0.49% were prepared, and they are denoted as Cu@TiO_2-A, Cu@TiO_2-B, Cu@TiO_2-C, Cu@TiO_2-D and Cu@TiO_2-E, respectively.

2.3. Characterization

The morphology of the Cu and Cu@TiO_2 nanostructures were observed using ZEISS SUPRA55VP scanning electron microscope (SEM). The microstructure of the Cu and Cu@TiO_2 nanostructures were studied with a HITACHI H-600 transmission electron microscope (TEM). UV–vis diffuse reflectance (DRS) of the samples was recorded by a Thermo Scientific Evolution 220 spectrometer. Electron paramagnetic resonance (EPR) spectra were recorded on a Bruker Elexsys E500 spectrometer. Surface composition analysis of Cu@TiO_2 was recorded using an ESCALAB Mark II X-ray photoelectron spectroscopy (XPS). The reactor was illuminated by a 350 W Xe lamp equipped with an ultraviolet cut-off filter (≥400 nm). The intensity of the light on sample system was measured to be 0.068 W/cm^2 by using a spectroradiometer. 2,4-dichlorophenol was sampled and the absorbance change at 282 nm was monitored using UV–vis spectroscopy (Shimadzu UV-1800).

3. Results and discussion

3.1. Characterization of the copper particles

Fig. 1 shows the time evolution of the UV–vis absorption spectra during the time course of preparation. Initially, no characteristic absorption peak is observed. After 2 h, the absorption peak around 320 nm emerges which was induced by the oxidation product of L-ascorbic. With the reaction progressing, the absorption peak gets intensive, and a second peak with comparable intensity shows up. The second peak is significantly red-shifted due to the growth of copper nanoparticles [15,16]. The whole synthesis process (including reduction reaction and Cu nanoparticles growth) was completed within 14 h as indicated by the fact that the UV–vis absorption spectra recorded after 14 h and 16 h are overlapped.

As shown in Fig. 2, the EDS spectrum only exhibits the characteristic peaks of Cu which means that the obtained product is composed of pure Cu.

3.2. Characterization of the Cu@TiO_2 nanoparticles

XRD patterns of the prepared Cu nanoparticles and Cu@TiO_2 products were shown in Fig. 3. High crystallinity is confirmed by the strong diffraction peaks. The diffraction peaks at 43.0, 50.1 and 74.4 are indexed to (1 1 1), (2 0 0) and (2 2 0) planes, respectively, which match well with the standard pattern of copper (JCPDS No. 03-1015). It is obvious that the Cu@TiO_2 nanocomposites with different Cu loadings exhibit similar XRD patterns. The peaks at 2θ values of 25.3, 37.8, 48.0, 53.9, 55.1, 62.7, 68.8, 70.3, and 75.0 can be indexed to (1 0 1), (0 0 4), (2 0 0), (1 0 5), (2 1 1), (2 0 4), (1 1 6), (2 2 0), and (2 1 5) crystal planes of anatase TiO_2 (JCPDS file: 010562), respectively. No typical diffraction peaks belonging to the Cu are observed in the Cu@TiO_2 core–shell nanocomposites. The reason

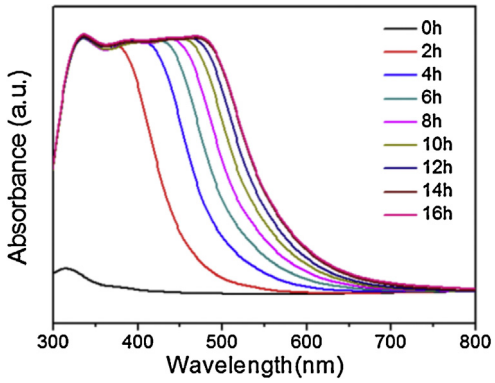

Fig. 1. Time evolution of the UV–vis absorption spectrum of as-prepared Cu nanoparticle solution.

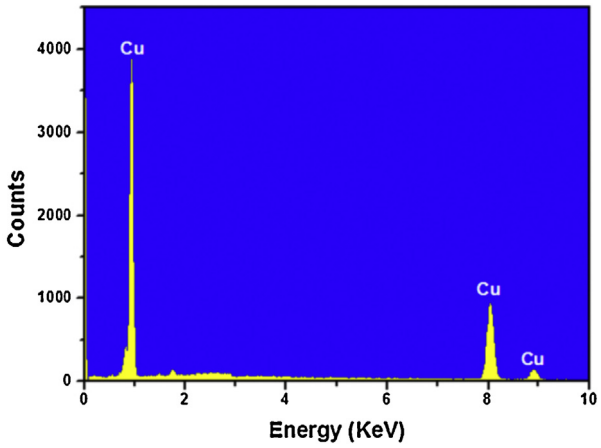

Fig. 2. EDS spectrum of the Cu nanoparticles stabilized in L-ascorbic acid aqueous solution.

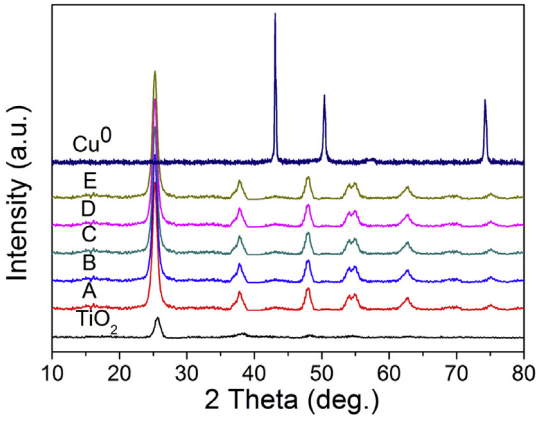

Fig. 3. XRD pattern of Cu nanoparticles (dispersed in the paraffin solution) and Cu@TiO_2 samples.

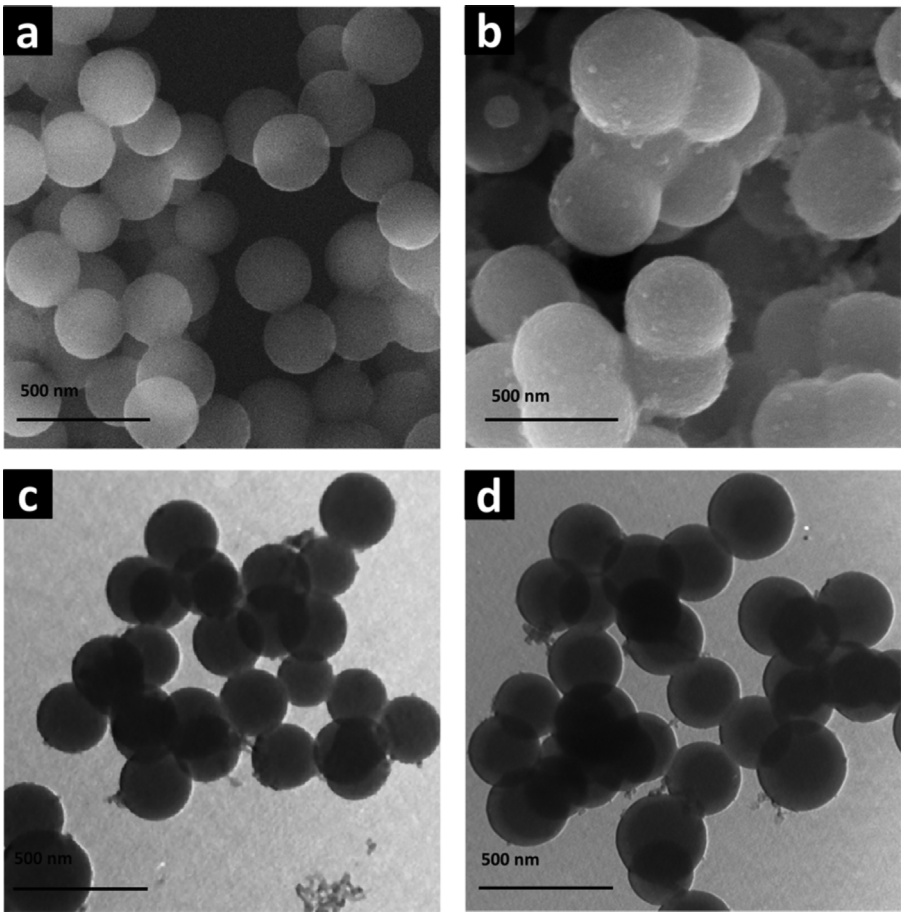

Fig. 4. SEM (a) and TEM (c) images of Cu nanoparticles; (b) and (d) are SEM and TEM images of the prepared Cu@TiO_2 nanoparticles with mass ratio of 1.07% (TiO_2:Cu).

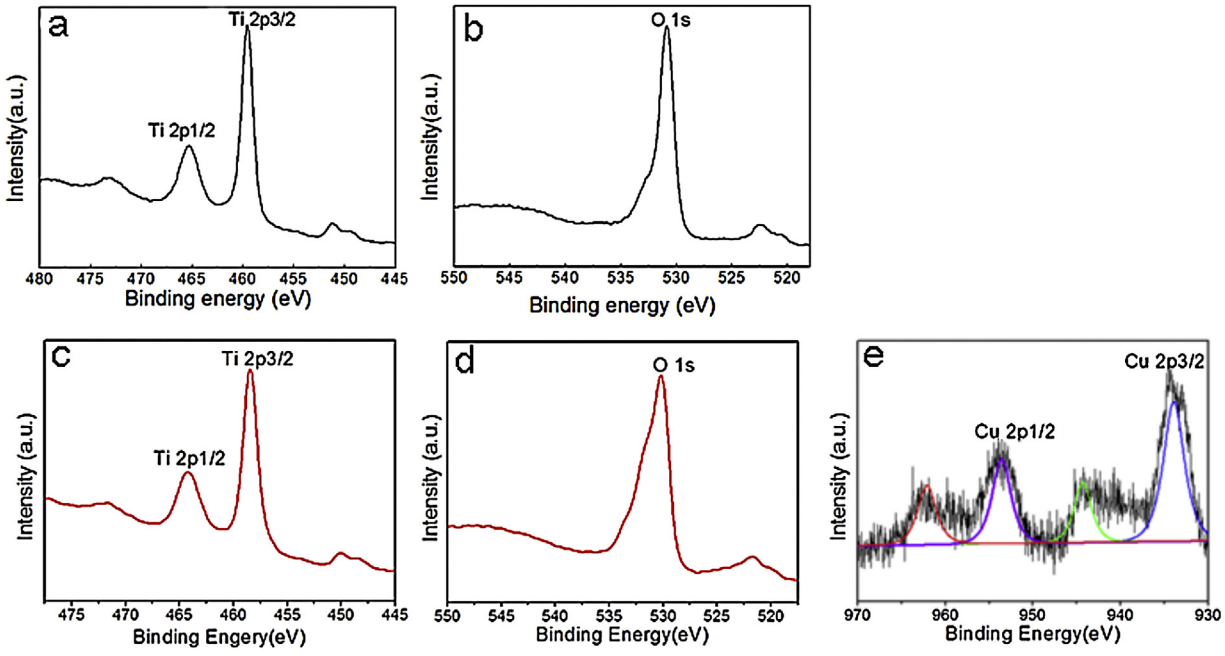

Fig. 5. XPS spectra of Ti 2p (a) and O 1s (b) in TiO_2 nanoparticles, and Ti 2p (c), O 1s (d), Cu 2p (e) in the Cu@TiO_2 nanoparticles.

can be ascribed to the even distribution and low weight loading of metal nanoparticles in the TiO_2.

Fig. 4a and b shows the SEM and TEM images of the Cu and Cu@TiO_2 samples as synthesized above. Both particles are in well-defined spherical shape. The average diameter of the Cu@TiO_2 composite particles is about 458 nm, while Cu core is about 375 nm and the TiO_2 shell is about 83 nm. Pure Cu nanoparticles before coupling with TiO_2 are basically solid sphere as shown in Fig. 4c.

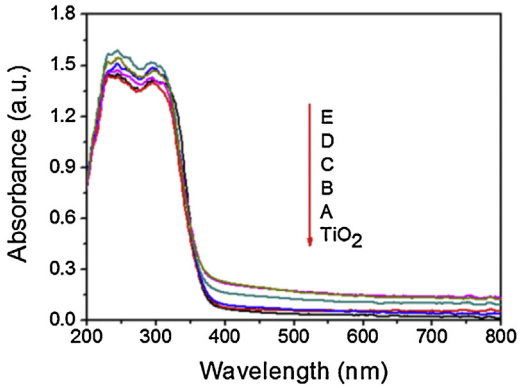

Fig. 6. UV–visible diffuse reflection spectra of Cu@TiO_2 with different mass ratio of $CuCl_2$ solution and TiO_2.

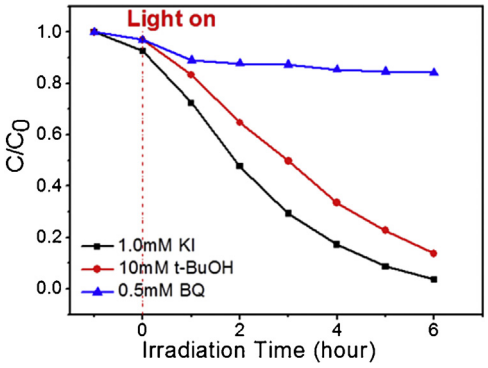

Fig. 9. Effects of I^-, *t*-BuOH and BQ on degradation of 2,4-DCP in the presence of Cu@TiO_2 under visible light irradiation.

The contrast between dark center and gray edge with the thickness is observed in Fig. 4d. This indicates that the Cu nanoparticles were successfully coated with the TiO_2 and further confirmed the formation of core–shell structure.

To investigate the chemical states of the elements in TiO_2 and Cu@TiO_2 samples, Ti 2p, O1 s and Cu 2p core levels were measured by XPS, and the results are presented in Fig. 5. As shown in Fig. 5a and b, for bared TiO_2, the XPS peaks of Ti 2p, Ti 2p1/2 (464.5 eV) and Ti 2p3/2 (458.3 eV) peaks are shown in Fig. 5a. The peak separation between the 2p1/2 and 2p3/2 lines is 6.2 eV, which are assigned to the Ti^{4+} oxidation state [17]. The XPS peak of O 1s in Fig. 5b is observed at 530.8 eV which is the characteristic of metallic oxides. For the Cu@TiO_2 nanoparticles, the XPS of the samples are mainly composed of Ti, O and Cu. With respect to the XPS peaks of Ti 2p in Fig. 5c, although there are slight differences in the locations of binding energies of Ti 2p1/2 and Ti 2p3/2 compared with the bared TiO_2, they are all still in good agreement with the values of Ti^{4+} [17]. The O 1s binding energies in Fig. 5d reveal lattice oxygen (530.0 eV) existing at the composite surface. These results further confirm the presence of TiO_2 at the composite surface [18]. The peaks observed at 952.55 eV and 932.6 eV (Fig. 5b) can be ascribed to Cu 2p1/2 and Cu 2p3/2 of the metallic copper [19] indicating that a certain quantity of encapsulated Cu nanoparticles must be naked after Ar^+ sputtered for 600 s. The peak can be fitted with the nonlinear least-squares fitting program using Gaussian–Lorentzian peak shapes [20]. Our results point out that Cu

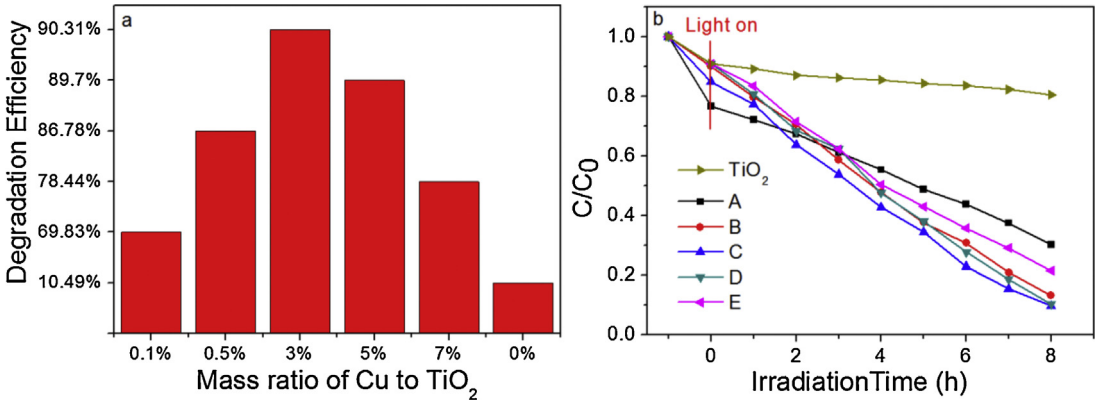

Fig. 7. Performances of Cu@TiO_2 core–shell nanoparticles for photocatalytic degradation of DCP under the irradiation of visible light.

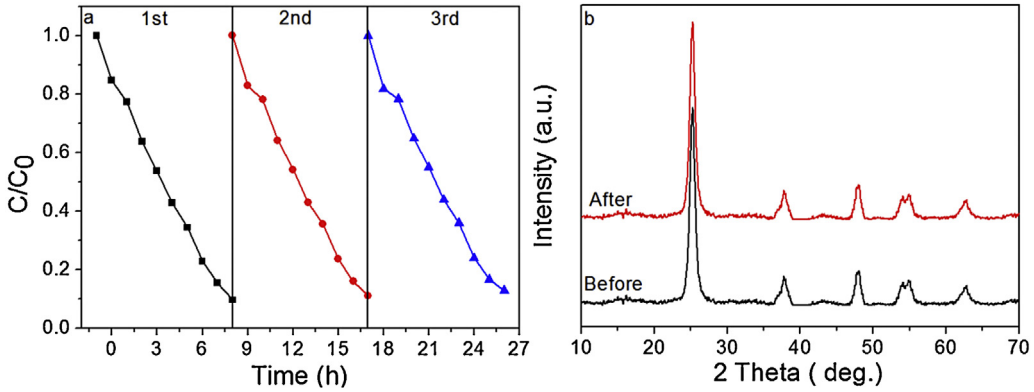

Fig. 8. (a) Photocatalytic stability of Cu@TiO_2 (mass ratios of 1.07%) in recycling reactions, (b) XRD partern of tested samples before and after three cycles in degradation of 2,4-DCP under under visible light irradiation.

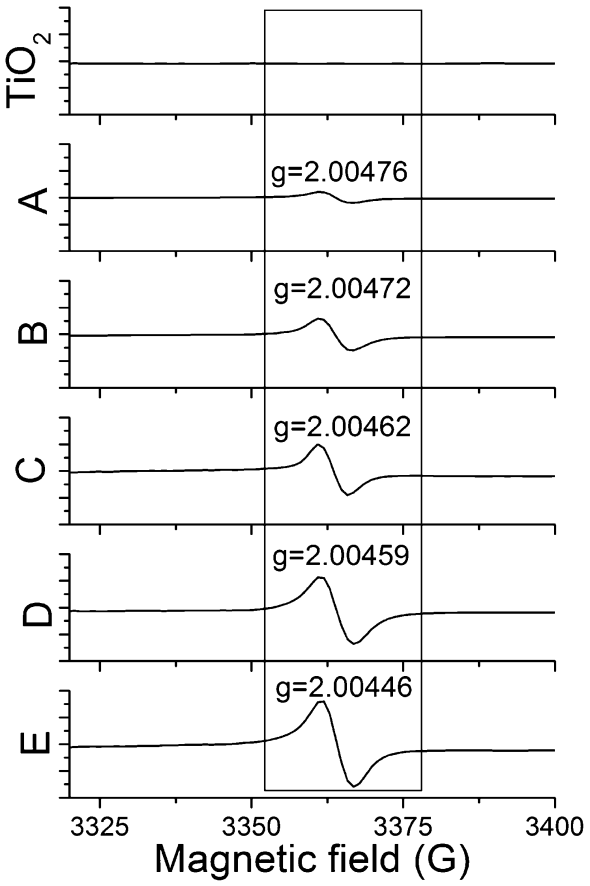

Fig. 10. EPR spectra (recorded at 298 K) of the Cu@TiO_2 core–shell nanoparticles.

nanoparticles were covered by TiO_2 and protected from oxidation as detected.

3.3. Optical and photocatalytic properties

UV–vis diffuse reflection spectra of Cu@TiO_2 with different mass ratios of Cu to TiO_2 compared with TiO_2 are displayed in Fig. 6. Compared with TiO_2, there is a critical point for mass ratio of TiO_2 to Cu when at around 1.53% where an enhancement of the visible-light absorption between 400 and 600 nm is generated [21]. The absorption intensity gradually strengthens with decrease in the mass ratio of TiO_2 to Cu.

Fig. 7 illustrates the photocatalytic activity of Cu@TiO_2 with different mass ratios for the degradation of 2,4-DCP under visible light irradiation. Without incorporation of Cu, the pure TiO_2 shows 10.49% degradation in visible light, while the photocatalytic performance of TiO_2 can be flexibly tuned by incorporation of different weights of Cu particles as shown in Fig. 7a and b, in which optimum performance is reached when the concentration of $CuCl_2$ solution is 4.75 mM. The degradation of 2,4-DCP can be fitted to a pseudo-first-order reaction with a simplified Langmuir–Hinshelwood model [22]. The variation of kinetic rate constant with the concentration of $CuCl_2$ solution follows the order C > D > B > E > A, and the corresponding value is 0.257 h^{-1}, 0.234 h^{-1}, 0.219 h^{-1}, 0.178 h^{-1} and 0.147 h^{-1}, respectively. Therefore, the incorporation of Cu plays an important role in the photocatalytic degradation process.

The tested sample retains photocatalytic activity after three successive cycles of complete degradation 2,4-DCP under visible light irradiation (Fig. 8). From Fig. 8a, it is clear that the degradation efficiency of Cu@TiO_2 core–shell nanoparticles almost maintains the same level as the original one and shows a minor reduction by about 3.2% after three cycles of 2,4-DCP degradation. Furthermore, from the XRD patterns, there is no obvious difference observed for the samples before and after the degradation reaction (Fig. 8b), further indicating the stability of the sample.

3.4. Mechanism for enhanced activity of Cu@TiO_2 core–shell nanoparticles

To explore the mechanism involved in Cu@TiO_2 photocatalysis, reactive species involved in the photocatalytic reaction was explored using *t*-BuOH, KI and benzoquinone (BQ) as scavenger of $HO^{\bullet}$, VB hole and $O_2^{\bullet-}$, respectively [23]. As can be seen from Fig. 9, excess KI shows a negligible effect on the photocatalytic oxidation of 2,4-DCP. Also, the degradation rate of 2,4-DCP is not affected by the addition of *t*-BuOH. However, the addition of excess BQ significantly inhibits the decomposition of 2,4-DCP compared with no scavenger at the same conditions, indicating that the 2,4-DCP photodegradation is proceeded by $O_2^{\bullet-}$ to a large degree [24].

The superoxide radicals $O_2^{\bullet-}$ discussed so far were further investigated by the electron paramagnetic resonance (EPR) (Fig. 10) spectrum recorded at room temperature confirming the significant presence of oxygen vacancies in the Cu@TiO_2, with a strong signal at $g = 2.004$ induced by electrons trapped on oxygen vacancies [25]. Without incorporated with the Cu, TiO_2 sample does not

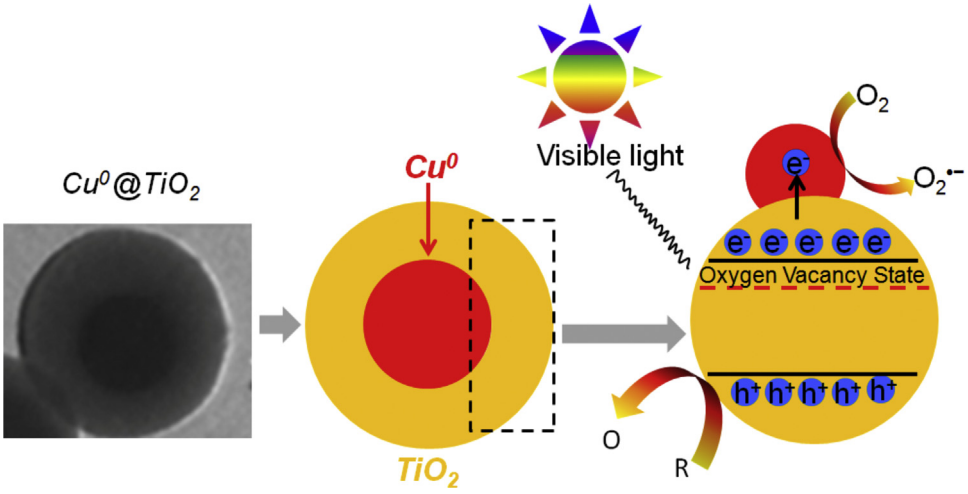

Scheme 1. Schematic diagram of electronic transition between TiO_2 and Cu under visible light irradiation.

contain any paramagnetic sites, as evidenced by a flat line shown in Fig. 10, whereas Cu@TiO_2 sample shows an intense signal at $g = 2.004$ shows up, which can be assigned to the single electron trapped on the oxygen vacancy states [26]. It should be noted that the oxygen vacancy formation does not accompany with the formation of Ti^{3+} defects, as can be seen from the X-ray photoelectron spectra (Fig. 5a), suggesting that almost no Ti^{3+} defects are formed during the oxygen vacancies formation [27]. The contribution of the signal at $g = 2.004$ steadily increases, since the O^{2-} species are affected by the content of the Cu. The relative intensities of the O^{2-} species follows the approximate trend of E > D > C > B > A, apart from the expected line broadening effects due to residual oxygen [28].

Based on the above observations, the mechanism of degradation of 2,4-DCP under visible light irradiation over Cu@TiO_2 is proposed as schematically presented in Scheme 1. It is believed that the core–shell structure of Cu@TiO_2 could favor charge transfer and inhibit recombination of photogenerated hole–electron pairs. Under the visible light excitation, the oxygen vacancy states can promote the visible-light absorption and the generation of the photoexcited electron–hole pairs over the surface of TiO_2 [29]. These photoexcited electrons and holes would suffer from both charge recombination and interfacial charge-transfer processes. Since Cu nanoparticles in the cores of Cu@TiO_2 nanospheres are good electron acceptors, they could promote the photoelectron transportation from TiO_2 shells and retard the recombination of photoexcited electron–holes on TiO_2 shells. Therefore, the efficiency toward photocatalytic redox process is improved. The adsorbed 2,4-DCP in solution interacts with photogenerated holes. In addition, the photogenerated electrons trapped by Cu particles can also be captured by oxygen, which produces superoxide radicals, as evidenced by the ESR analysis. These oxygen-containing species (O_2 or $O_2^{\bullet -}$) then are able to oxidize the 2,4-DCP.

4. Conclusions

The present study demonstrates that Cu@TiO_2 core–shell nanoparticles have been successfully fabricated via a facile in situ hydrolysis method. The incorporation of Cu core into the shell of TiO_2 contributes to the enhancement of visible light photocatalytic activity of TiO_2. The oxygen vacancy states can promote the visible-light absorption and the generation of the photoexcited electron–hole pairs over the surface of TiO_2. The enhanced photoactivity lies crucially on the contribution role of Cu nanoparticles acting as electron reservoir in prolonging the lifetime of photogenerated charge carriers. The reaction mechanism of the photocatalytic reaction over Cu@TiO_2 is also proposed by using different radical scavengers and EPR analysis. It is hoped that the present work could render guided information for steering toward the design and application of Cu@TiO_2 core–shell nanoparticles with visible light driven photocatalytic activity.

Acknowledgements

This work was supported by the National Nature Science Foundation of China (Grant No. 21173261), the CAS/SAFEA International Partnership Program for Creative Research Teams, the CAS Cross-Cooperation Program for Creative Research Teams, the CAS "Western Action Plan" (KGZD-EW-502), the "Western Light" (XBBS 201126) of Chinese Academy of Sciences, and the "Youth Technology Innovation Talents Culture Engineering" of Xinjiang Uygur Autonomous Region of China (no. 2013721045).

References

[1] H.G. Yang, C.H. Sun, S.Z. Qiao, Nature 453 (2008) 638.
[2] X. Fan, L. Zang, M. Zhang, H. Qiu, Z. Wang, J. Yin, H. Jia, S. Pan, C. Wang, Chem. Mater. 26 (2014) 3169.
[3] X. Fan, K. Lai, L. Wang, H. Qiu, J. Yin, P. Zhao, S. Pan, J. Xu, C. Wang, J. Mater. Chem. A 3 (2015) 12179.
[4] J. Yu, J. Low, W. Xiao, P. Zhou, M. Jaroniec, J. Am. Chem. Soc. 136 (2014) 8839.
[5] Z. Li, Y. Qu, G. He, M. Humayun, S. Chen, L. Jing, Appl. Surf. Sci. 351 (2015) 681.
[6] R.T. Ako, P. Ekanayake, D.J. Young, J. Hobley, V. Chellappan, A.L. Tan, S. Gorelik, G.S. Subramanian, C.M. Lim, Appl. Surf. Sci. 351 (2015) 950.
[7] M.M. Momeni, Y. Ghayeb, Z. Ghonchegi, Ceram. Int. 41 (2015) 8735.
[8] Y. Li, B. Wang, S. Liu, X. Duan, Z. Hu, Appl. Surf. Sci. 324 (2015) 736.
[9] N.A. Dhas, C.P. Raj, A. Gedanken, Chem. Mater. 10 (1998) 1446.
[10] C. Wang, Q. Hu, J. Huang, C. Zhu, Z. Deng, H. Shi, L. Wu, Z. Liu, Y. Cao, Appl. Surf. Sci. 292 (2014) 161.
[11] H.M. Yadav, S.V. Otari, V.B. Koli, S.S. Mali, C.K. Hong, S.H. Pawar, S.D. Delekar, J. Photochem. Photobiol. A 280 (2014) 32.
[12] S.H. Sun, C.B. Murray, D. Weller, L. Folks, A. Moser, Science 278 (2000) 1989.
[13] I. Ganesh, P.P. Kumar, I. Annapoorna, J.M. Sumliner, M. Ramakrishna, N.Y. Hebalkar, G. Padmanabham, G. Sundararajan, Appl. Surf. Sci. 293 (2014) 229.
[14] J. Xiong, Y. Wang, Q. Xue, X. Wu, Green Chem. 4 (2011) 900.
[15] S.G. Kumar, L.G. Devi, J. Phys. Chem. A 115 (2011) 13211.
[16] I. Pastoriza-Santos, A. Sánchez-Iglesias, B. Rodíguez-González, L.M. Liz-Marzán, Small 5 (2009) 440.
[17] H.G. Yang, H.C. Zeng, J. Phys. Chem. B 108 (2004) 3492.
[18] N. Zhang, S.Q. Liu, X.Z. Fu, Y.J. Xu, J. Phys. Chem. C 115 (2011) 9136.
[19] J. Fu, S. Cao, J. Yu, J. Materiomics 1 (2015) 124.
[20] J. Yu, Y. Hai, M. Jaroniec, J. Colloid Interface Sci. 357 (2011) 223.
[21] Z.H. Zhang, L.B. Zhang, M.N. Hedhili, H.N. Zhang, P. Wang, Nano Lett. 13 (2013) 14.
[22] B. Bayarrioe, J. Gimeaenez, D. Curcoae, S. Esplugas, Catal. Today 101 (2005) 227.
[23] Y.Y. Li, J.S. Wang, H.C. Yao, L.Y. Dang, Z.J. Li, J. Mol. Catal. A: Chem. 334 (2011) 116.
[24] P.D. Cozzoli, M.L. Currib, A. Agostiano, Chem. Commun. 25 (2005) 3186.
[25] X. Pan, M.-Q. Yang, X. Fu, N. Zhang, Y.-J. Xu, Nanoscale 5 (2013) 3601.
[26] R. Li, H. Kobayashi, J. Guo, J. Fan, Chem. Commun. 47 (2011) 8584.
[27] X. Pan, Y.-J. Xu, J. Phys. Chem. C 117 (2013) 17996.
[28] E. Carter, A.F. Carley, D.M. Murphy, J. Phys. Chem. C 111 (2007) 10630.
[29] A. Naldoni, M. Allieta, S. Santangelo, M. Marelli, F. Fabbri, S. Cappelli, C.L. Bianchi, R. Psaro, V. Dal Santo, J. Am. Chem. Soc. 134 (2012) 7600.